Aeroacoustics Conferences
June 14-17, 2022, Southampton, UK
28th AIAA/CEAS Aeroacoustics 2022 Conference

10.2514/6.2022-2870

Effects of the upstream-propagating guided jet waves on the mixing layers of Mach number 0.9 free jets

Christophe Bogey*
Univ Lyon, CNRS, Ecole Centrale de Lyon, INSA Lyon, Univ Claude Bernard Lyon I,
Laboratoire de Mécanique des Fluides et d'Acoustique, UMR 5509, 69130 Ecully, France

The effects of the upstream-propagating guided jet waves on the mixing layers of free isothermal jets at a Mach number of 0.9 are investigated for four jets computed using large-eddy simulations, three ones with laminar nozzle-exit boundary layers and one with disturbed boundary layers. For the initially laminar jets, the velocity spectra obtained in the mixing layers upstream and downstream of the first stage of vortex pairings are dominated by multiple peaks associated with the azimuthal modes n_θ = 0, 1 and 2. For the dominant peaks and most other ones, the frequencies are located inside or near the frequency bands of the free-stream upstream-propagating guided jet waves. In this case, standing-wave patterns are found in the root-mean-square fluctuation fields on both sides of the shear layers. Otherwise, the peak frequencies are harmonics of the frequency of the dominant peak. Therefore, the guided jet waves not only excite the Kelvin-Helmholtz instability waves growing close to the nozzle [1], but also govern the mixing-layer development farther downstream during the laminar-turbulent transition. For the initially disturbed jet, the velocity spectra in the mixing layers are broadband. For n_θ = 0, however, one small peak seems to appear several diameters downstream of the nozzle. This peak is at a Strouhal number approximately of 0.41, similar to that of the tone emerging in the near-nozzle pressure spectra in the frequency band of the first radial mode of the free-stream upstream-propagating guided jet waves. This suggests that the turbulent structures of the jet mixing layers are affected by the guided jet waves at this frequency.

I. Introduction

There has been considerable progress in the last years in the prediction and understanding of jet noise generation mechanisms, as pointed out in the reviews of Brès and Lele [2] and Lyrintzis and Coderoni [3], for instance. In particular, a number of studies, collected in Edgington-Mitchell [4], have emphasized the crucial role of the guided jet waves in the establishment of resonance phenomena in jets. These guided jet waves, first described as neutral acoustic waves in Tam and Hu [5], are essentially confined inside the jet flow. Among them, those travelling in the upstream direction with a significant amplitude not only in the jet potential core but also in the shear layer and outside the jet are especially important. These waves, named as free-stream upstream-propagating guided jet waves in Towne et al. [6], are only allowed in narrow frequency bands. They have been found to close the feedback loops occurring in subsonic and supersonic ideally-expanded impinging jets in Tam and Ahuja [7], Tam and Norum [8], Gojon et al. [9] and Bogey and Gojon [10]. As a result, the frequencies and axisymmetric or helical natures of the tones observed in such flow configurations can be explained by the dispersion relations and modal classification of these waves. Similar results have been obtained for jet-flap interaction tones by Jordan et al. [11] and Tam and Chandramouli [12] and for the screech tones emitted by non-ideally expanded supersonic jets by Shen and Tam [13], Gojon et al. [14], Edgington-Mitchell et al. [15] and Mancinelli et al. [16]. For high subsonic and ideally expanded supersonic jets, the upstream-propagating guided jet waves also lead to the generation of acoustic tones in the potential core, as shown in Towne et al. [6] and Schmidt et al. [17], as well as in the near-nozzle region and in the upstream far field, as reported in Suzuki and Colonius [18], Brès et al. [19], Bogey [20], Zaman et al. [21] and Bogey [22], among others.

Several question remain about the effects of the guided jet waves on the turbulent development and noise generation mechanisms of free jets containing no shocks. The influence of the upstream-propagating guided jet waves on the Kelvin-Helmholtz instability waves initially growing downstream of the nozzle lip was investigated recently in Bogey [1] for isothermal free jets at Mach numbers M between 0.50 and 2 with fully laminar or highly disturbed nozzle-exit boundary layers using large-eddy simulations (LES). For laminar boundary layers, the velocity spectra obtained on the nozzle-lip line at axial positions corresponding roughly to the rolling-up of the shear layers contain strong peaks

*CNRS Research Scientist, christophe.bogey@ec-lyon.fr, AIAA Senior Member & Associate Fellow.

associated with the azimuthal modes $n_\theta = 0$, 1 and 2. The peak frequencies are close to those of the most amplified instability waves predicted from the mean flow profiles using linear stability analysis, as expected given the results in Michalke [23] and Morris [24], for instance. More surprisingly, they fall within the frequency bands of the free-stream upstream-propagating guided jet waves and jump from one band to another as the Mach number increases. These results indicate that the jet initial instability waves are excited by the waves mentioned above, as in screeching and impinging resonant jets. This provides an explanation for the disparities in the frequency and azimuthal mode dominating early on in the shear layers of initially laminar jets, illustrated by the experimental data gathered in Gutmark and Ho [25], and for their discontinuous changes as the jet velocity varies. For disturbed boundary layers, the velocity spectra just downstream of the nozzle lip have broadband shapes centered around the most unstable frequency. The finding of standing-wave patterns at the frequencies of the free-stream upstream-propagating guided jet waves and of significant correlations between near-nozzle and shear-layer fluctuations, however, suggests the possibility of interactions between guided jet waves and Kelvin-Helmholtz instability waves near the nozzle of jets for $M \geq 0.90$.

In the present study, as an extension of the work above, the influence of the free-stream upstream-propagating guided jet waves on the mixing layers of isothermal free jets is investigated well downstream of the nozzle in regions where the amplitudes of the instability waves initially growing near the nozzle have saturated and eventually decayed. Among the several dozen of jets computed by LES in Bogey [1, 20], four jets at a Mach number of 0.9 are considered. At the nozzle exit, three ones have fully laminar boundary layers of different thickness and the fourth one has highly disturbed boundary layers. The objective will be to examine how much and how far from the nozzle the guided jet waves affect the jet mixing-layer development for the two exit flow conditions. In particular, the questions will be to determine whether the effects of the free-stream upstream-propagating guided jet waves persist all over the laminar-turbulent flow transition region in the laminar case, and whether they can be detected several diameters from the nozzle in the disturbed case. For that purpose, the properties of the velocity disturbances in the mixing layers, notably their frequency contents and azimuthal structures, will be detailed. They will be compared with the results obtained using linear stability analysis from the LES mean flow profiles, with the characteristics of the free-stream upstream-propagating guided jet waves provided by a vortex-sheet model and with the properties of the acoustic tones near the nozzle. The presence of standing-wave patterns, which can result from the interactions between upstream-propagating and downstream-propagating waves, as highlighted in Panda [26] for screeching jets, for instance, will also be checked in the root-mean-square (r.m.s.) fluctuation flow fields at specific frequencies.

The paper is organized as follows. In section II, the jet initial conditions and the LES methods and parameters are documented. In section III, vorticity and pressure snapshots are first shown. Then, the characteristics of the velocity fields obtained in the mixing layers of the jets with untripped and tripped boundary layers are presented and discussed. Finally, concluding remarks are given in section IV.

II. Parameters

A. Jet flow conditions

Four isothermal round jets at a Mach number $M = u_j/c_0$ of 0.9 and a Reynolds number $Re_D = u_j D/\nu$ of 10^5, where u_j, c_0, D and ν are the jet exit velocity, the speed of sound in the ambient medium, the nozzle diameter and the kinematic molecular viscosity, are considered in this study. They originate from a pipe nozzle of radius $r_0 = D/2$ and length $2r_0$ into a medium at ambient temperature and pressure $T_0 = 293$ K and $p_0 = 10^5$ Pa. The pipe exit is at $z = 0$, and the pipe-wall thickness is $0.053r_0$. At the pipe inlet, at $z = -2r_0$, Blasius laminar boundary-layer profiles of thickness δ_{BL} are imposed for the axial velocity [27]. Radial and azimuthal velocities are set to zero, pressure is equal to p_0, and temperature is determined by a Crocco-Busemann relation. Results obtained for the four jets, including their nozzle-exit mean and r.m.s. velocity profiles, can be found in several previous papers [1, 20, 28, 29].

For the first three jets, the boundary layers have thicknesses of $\delta_{BL} = 0.05r_0$, $0.1r_0$ and $0.2r_0$ at the pipe inlet and are untripped in the nozzle. As a consequence, the nozzle-exit mean velocity profiles resemble the pipe-inlet Blasius profiles and are characterized by momentum thicknesses of $\delta_\theta = 0.007r_0$ for $\delta_{BL} = 0.05r_0$, $\delta_\theta = 0.012r_0$ for $\delta_{BL} = 0.1r_0$ and $\delta_\theta = 0.024r_0$ for $\delta_{BL} = 0.2r_0$. For comparison, Zaman [30] measured $\delta_\theta = 0.0062r_0$ in an untripped jet at $Re_D = 10^5$. With respect to this jet, the boundary layer has a similar thickness for the jet with $\delta_{BL} = 0.05r_0$ and is thicker for $\delta_{BL} \geq 0.1r_0$. As for the velocity fluctuations, their peak r.m.s. values u'_e at the nozzle exit do not exceed $0.002u_j$, indicating that the jets are initially fully laminar. In order to trigger the formation of vortical structures in the jets, which would, otherwise, remain laminar over very long time periods due to the absence of boundary-layer tripping, pressure fluctuations of maximum amplitude 200 Pa random in both space and time are introduced in the

shear layers between $z = 0.25r_0$ and $z = 4r_0$ from $t = 0$ up to $t = 12.5r_0/u_j$. Afterwards, the jets develop without any external forcing.

For the fourth jet, the boundary layers are $\delta_{BL} = 0.15r_0$ thick at the pipe inlet and are tripped by adding random low-level vortical disturbances uncorrelated in the azimuthal direction in the pipe [31] in order to generate turbulent structures typical of those encountered in wall-bounded flows [32]. The forcing is applied at the axial position $z = -0.95r_0$ and the radial position $r = r_0 - \delta_{BL}/2$ with a magnitude adjusted to obtain the desired level of peak turbulence intensity in the pipe-exit section. In this plane, the mean velocity profile is similar to a laminar boundary-layer profile of momentum thickness $\delta_\theta = 0.018r_0$, while the r.m.s. velocity profile reaches a peak value approximately of $0.09u_j$, indicating that the jet is initially highly disturbed. That was also the case in the experiments of Zaman [30] for a tripped jet at $\mathrm{Re}_D = 10^5$.

B. Numerical methods

The jets are computed by LES using the same framework as in previous jet simulations [27, 31, 33–35]. The LES are carried out by solving the three-dimensional compressible Navier-Stokes equations in cylindrical coordinates (r, θ, z) using low-dissipation and low-dispersion explicit schemes. The axis singularity is taken into account by the method of Mohseni and Colonius [36]. In order to alleviate the time-step restriction near the cylindrical origin, the derivatives in the azimuthal direction around the axis are calculated at coarser resolutions than permitted by the grid [37]. For the points closest to the jet axis, they are evaluated using 16 points, yielding an effective resolution of $2\pi/16$. Fourth-order eleven-point centered finite differences are used for spatial discretization and a second-order six-stage Runge-Kutta algorithm is implemented for time integration [38]. A sixth-order eleven-point centered filter [39] is applied explicitly to the flow variables every time step. Non-centered finite differences and filters are also used near the pipe walls and the grid boundaries [27, 40]. At the boundaries, the radiation conditions of Tam and Dong [41] are applied, with the addition at the outflow of a sponge zone combining grid stretching and Laplacian filtering in order to avoid significant acoustic reflections. Small adjustment terms are also added to prevent that mean density and pressure deviate significantly from ambient density and pressure, and no co-flow is imposed. In the present simulations, the explicit filtering is employed to remove grid-to-grid oscillations, but also, as the mesh grid is not fine enough to compute the smallest turbulent structures, as a subgrid-scale high-order dissipation model in order to relax turbulent energy from scales at wave numbers close to the grid cut-off wave number while leaving larger scales mostly unaffected. The performance of this large-eddy simulation (LES) approach has been assessed in past studies for subsonic jets, Taylor-Green vortices and turbulent channel flows [42–44].

C. Simulation parameters

The same mesh grid is used in the (r, z) section in the four jet simulations. It was constructed in a previous grid-sensitivity study [34] carried out for the present untripped jet with $\delta_{BL} = 0.2r_0$ and for the tripped jet. It contains $N_r = 512$ points in the radial direction and $N_z = 2085$ points in the axial direction. Its physical extents are $L_r = 15r_0$ and $L_z = 40r_0$. The minimum mesh spacings are equal to $\Delta r = 0.0036r_0$ at $r = r_0$ and $\Delta z = 0.0072r_0$ at $z = 0$. The maximal mesh spacing in the jet near field is equal to $\Delta r = 0.075r_0$, leading to a Strouhal number of $\mathrm{St}_D = fD/u_j = 5.9$ for an acoustic wave discretized by five points per wavelength, where f is the frequency. In the azimuthal direction, there are $N_\theta = 256$ points for the untripped jet with $\delta_{BL} = 0.2r_0$, $N_\theta = 512$ points for the untripped jets with $\delta_{BL} = 0.1r_0$ and $0.05r_0$ and $N_\theta = 1024$ points for the tripped jet. Approximately 50 GB, 100 GB and 200GB of memory are required, respectively.

The simulations have been performed with an OpenMP-based in-house solver using a time step Δt of $0.7 \times \Delta r(r = r_0)/c_0$ in order to ensure numerical stability. The simulation time T after the transient period is equal to $1000r_0/u_j$ for the untripped jets with $\delta_{BL} = 0.1r_0$ and $0.05r_0$, to $3000r_0/u_j$ for the untripped jet with $\delta_{BL} = 0.2r_0$ and to $3625r_0/u_j$ for the tripped jet. During time T, density, velocity components and pressure have been recorded at several locations, refer for instance to Bogey [45] for an exhaustive description of the data available. The data of interest in this work include those on the cylindrical surface located at $r = r_0$, which have been stored at a sampling frequency allowing spectra to be computed up to $\mathrm{St}_D = 12.8$. The signals have also been acquired in the azimuthal planes at the four angles between $\theta = 0$ and $3\pi/2$ every $\pi/2$ for the untripped jets and at the eight angles between $\theta = 0$ and $7\pi/4$ every $\pi/4$ for the tripped jet at a sampling frequency of $\mathrm{St}_D = 6.4$. The Fourier coefficients estimated over the full section (r, z) for the first nine azimuthal modes for density, velocity components and pressure have been similarly saved. The statistics are averaged in the azimuthal direction, when possible. The time spectra are evaluated from overlapping samples of duration $90r_0/u_j$ otherwise.

D. Vortex-sheet model and linear stability analysis

In order to discuss the possible interactions between the guided jet waves and the shear-layer velocity fluctuations of the jets, the LES results will be compared with the properties of the free-stream upstream-propagating guided jet waves provided by a vortex-sheet model and with the most unstable frequencies predicted using linear stability analysis from the jet mean flow fields in the next section.

The properties of the free-stream upstream propagating guided jet waves are obtained from the dispersion relations and eigenfunctions of the guided jet waves give by a vortex-sheet model, following Tam and Hu [5] and Morris [24], among others. This model making use of the assumption of an infinitely thin shear layer, differences can be expected with respect to the LES results for jets with mixing layers of finite width. They should, however, be small given the results available in the literature [1, 7, 20]. Remind that among the guided jet waves, the free-stream upstream-propagating ones are those travelling in the upstream direction with a significant amplitude in the shear layer and outside the jet [6]. They can only exist in narrow frequency bands, represented in Bogey [1].

The linear stability analysis is conducted from the jet mean flow fields, as was done in previous studies [1, 19, 46]. The procedure used is that recently developed to investigate the influence of the nozzle-exit boundary-layer profile on high-subsonic jets [35, 47]. For a given axial distance between $z = 0.02r_0$ and $5r_0$ for the untripped jets and between $z = 0.02r_0$ and $12r_0$ for the tripped jet, and for a given Strouhal number St_D, the compressible Rayleigh equation [23] is solved through a shooting technique [24] for the azimuthal modes $n_\theta = 0$, 1 and 2. The integration is performed directly from the LES mean velocity and density profiles, interpolated on a grid extending from $r = 0$ to $3r_0$ every $0.0005r_0$ and then smoothed using a high-order centered filter in order to remove spurious high-frequency oscillations. Viscous effects are not taken into account.

III. Results

A. Vorticity and pressure snapshots

Fields of the vorticity norm and of the pressure fluctuations obtained in the (z,r) plane downstream of nozzle for the jets with untripped boundary layers with $\delta_{BL} = 0.2r_0$ and $\delta_{BL} = 0.1r_0$ and for the jet with tripped boundary layers are represented in figures 1(a-c). For the two initially laminar jets, in figures 1(a,b), the shear layers roll up more rapidly and vortical structures form farther upstream as the thickness of the nozzle-exit boundary layer decreases, as expected [27, 34]. A first stage of vortex pairings is also clearly observed, around $z = 4r_0$ for $\delta_{BL} = 0.2r_0$ and $z = 2.5r_0$ for $\delta_{BL} = 0.1r_0$. For the untripped jet with $\delta_{BL} = 0.05r_0$, not shown for brevity, it occurs around $z = 1.5r_0$. For the initially highly disturbed jet, in figure 1(c), turbulent disturbances are found just downstream of the nozzle and no vortex pairing can be easily detected in the mixing layers. In the near pressure fields, low-frequency hydrodynamic waves are visible in the vicinity of the flow large-scale structures in all cases. Acoustic waves, including waves propagating in the upstream direction inside and outside of the jet potential core, also appear. These upstream-travelling waves generate acoustic tones in the pressure spectra in the potential core and outside near the nozzle lip [6, 19, 21], at frequencies falling in the ranges of the free-stream upstream propagating guided jet waves. The characteristics of the tones obtained for the present jets are detailed in Bogey [20].

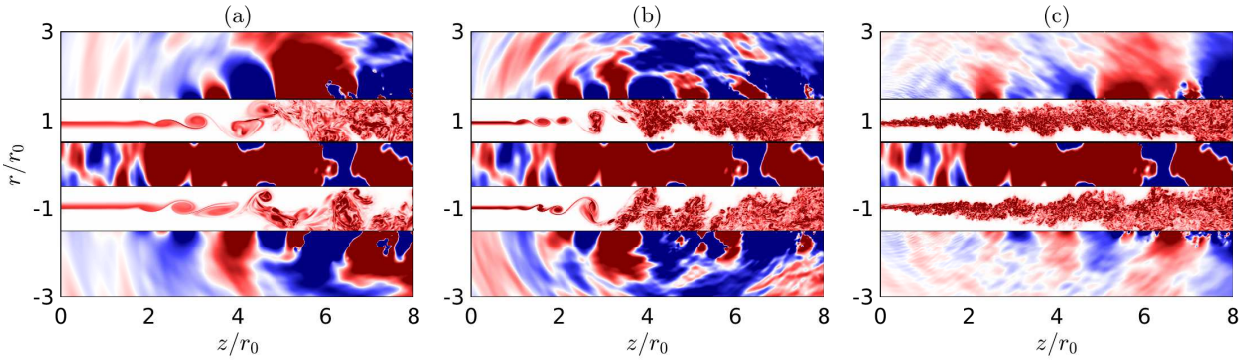

Fig. 1 Vorticity norm in the flow and pressure fluctuations outside for the jets (a,b) with untripped boundary layers with $\delta_{BL} = 0.2r_0$ and $\delta_{BL} = 0.1r_0$ and (c) with tripped boundary layers. The color scales range between $\pm 15u_j/r_0$ and ±475 Pa, from blue to red.

B. Mixing-layer development

The interactions between the upstream-propagating guided jet waves and the initial Kelvin-Helmholtz instability waves in the present jets have been recently investigated [1], notably by calculating velocity spectra at $r = r_0$ just downstream of the nozzle lip. For the untripped jets, the spectra were computed at $z = 100\delta_\theta(z = 0)$ near the shear-layer rolling-up, where $\delta_\theta(z = 0)$ is the boundary-layer momentum thickness at the nozzle exit, yielding $z = 0.74r_0$ for $\delta_{BL} = 0.05r_0$, $z = 1.23r_0$ for $\delta_{BL} = 0.1r_0$ and $z = 2.34r_0$ for $\delta_{BL} = 0.2r_0$. For the tripped jet, the spectra were estimated at $z = 0.4r_0$ very close to the nozzle. The peak frequencies obtained for the first three azimuthal modes are represented in figures 2(a-c) as a function of δ_{BL}/r_0.

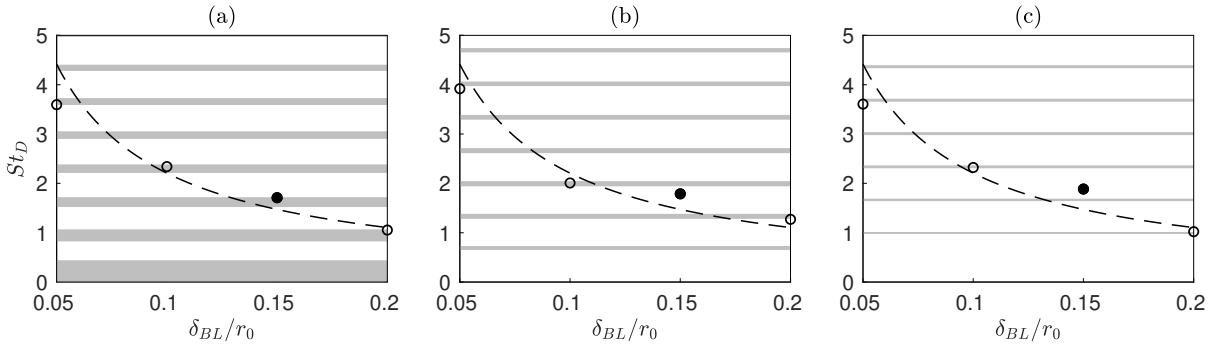

Fig. 2 Peak Strouhal numbers in the spectra of radial velocity fluctuations at $r = r_0$ for (a) $n_\theta = 0$, (b) $n_\theta = 1$ and (c) $n_\theta = 2$ as a function of δ_{BL}/r_0: $\circ$ at $z = 100\delta_\theta(0)$ for the untripped jets and $\bullet$ at $z = 0.4r_0$ for the untripped jet; (grey) frequency ranges of the free-stream upstream-propagating guided jet waves; $- - -$ $f\delta_\theta(0)/u_j \simeq 0.013$.

For the untripped jets, narrow peaks appeared to strongly emerge in the spectra, at frequencies similar to the mixing-layer most unstable frequency, approximated by $f\delta_\theta(0)/u_j = 0.013$ in the figures. More importantly, these frequencies lie inside or very near the bands of the free-stream upstream-propagating guided jet waves, in grey, indicating that the initial Kelvin-Helmholtz instability waves are excited by the latter waves. For the tripped jet, the spectra were found to be mainly broadband. For the axisymmetric mode, however, small peaks were obtained at $\mathrm{St}_D = 0.416$ and at $\mathrm{St}_D = 0.671$. Moreover, as shown in figure 2(a), the Strouhal number $\mathrm{St}_D = 1.709$ of the dominant components is close to the band of the third radial mode of the free-stream upstream-propagating guided jet waves, suggesting the possibility of interactions between these waves and the instability waves just downstream of the nozzle. This assertion is also supported by the presence of standing-wave patterns in the r.m.s. fluctuating flow fields at this frequency between $z = 0$ and $z = 3r_0$ at the edges of the mixing layer [1].

The question of whether the upstream-propagating guided jet waves affect the mixing-layer development at larger axial distances, namely downstream of the shear-layer rolling-up for the untripped jets and several diameters downstream of the nozzle for the tripped jet, is addressed in what follows.

1. Jets with untripped boundary layers

To quantity the laminar-turbulent transition in the mixing layers of the three jets with untripped boundary layers, the r.m.s. values of radial velocity fluctuations obtained at $r = r_0$ between $z = 0$ and $z = 8r_0$ are presented in figures 3(a-c). The values computed for the modes $n_\theta = 0$, 1 and 2 and the positions $z = 100\delta_\theta(0)$ are also displayed. The total levels rapidly increase and reach strong peak values greater than 20 per cent of the jet exit velocity, as expected for initially laminar flow conditions [48, 49]. Obviously, the peak moves closer to the nozzle exit for a thinner boundary layer, from $z \simeq 5r_0$ for $\delta_{BL} = 0.2r_0$ up to $z \simeq 1.8r_0$ for $\delta_{BL} = 0.05r_0$. In addition, the profiles exhibit dual-peak shapes, which can be attributed to a first stage of vortex pairings happening at a location that does not vary much [27, 50].

Regarding the contributions of modes $n_\theta = 0$, 1 and 2, they are significant for all jets. However, significant differences can be noted between the three cases in terms of levels and axial variations. For $\delta_{BL} = 0.2r_0$, in figure 3(a), mode $n_\theta = 1$ is initially the most amplified, but the strongest peak value is obtained for mode $n_\theta = 0$, and the peak for mode $n_\theta = 2$ is located approximately one diameter downstream compared with the two other modes. For $\delta_{BL} = 0.1r_0$, in figure 3(b), mode $n_\theta = 1$ predominates all along the laminar-turbulent transition. Finally, for $\delta_{BL} = 0.05r_0$, in figure 3(c), mode $n_\theta = 1$ is also dominant, but its contribution is just slightly higher than that for mode $n_\theta = 2$.

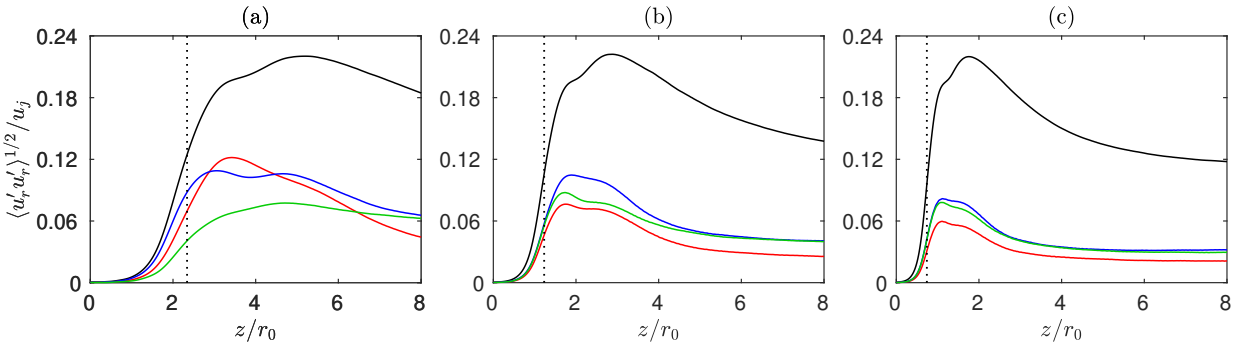

Fig. 3 Variations of the r.m.s. values of radial velocity fluctuations at $r = r_0$ for the jets with untripped boundary layers with (a) $\delta_{BL} = 0.2r_0$, (b) $\delta_{BL} = 0.1r_0$ and (c) $\delta_{BL} = 0.05r_0$: ——— full signals, ——— $n_\theta = 0$, ——— $n_\theta = 1$ and ——— $n_\theta = 2$; ····· $z = 100\delta_\theta(0)$.

The spectra of radial velocity fluctuations calculated at $r = r_0$ for the three untripped jets are represented in figures 4(a-c) as a function of z/r_0 and St_D. The most unstable frequencies predicted from the mean flow fields using linear stability analysis for $n_\theta = 0$ and the values and half the values of the peak frequencies in the spectrograms are also shown. Overall, due to the mixing-layer spreading, the frequencies of the velocity components decrease with the axial position, following the variations of the most unstable frequency with an axial shift of the order of r_0. Peaks are found to emerge at specific frequencies and to persist over large distances well downstream of $z = 100\delta_\theta(0)$. For $\delta_{BL} = 0.2r_0$ in figure 4(a), for instance, two spots of peak values are first visible between $z \simeq 2r_0$ and $4r_0$ at $\mathrm{St}_D \simeq 1$ and 1.3, close to the most unstable Strouhal numbers obtained near the nozzle exit. Farther downstream, between $z \simeq 3r_0$ and $5r_0$, two regions of high values can be seen at frequencies approximately twice lower than those mentioned above, as typically observed after the occurrence of vortex pairings. Finally, for $z > 6r_0$, the spectra are rather broadband and peaks do not clearly appear as turbulence is developed in the mixing layers. For a thinner exit boundary layer, in figures 4(b,c), there are more peaks but they seem to be weaker.

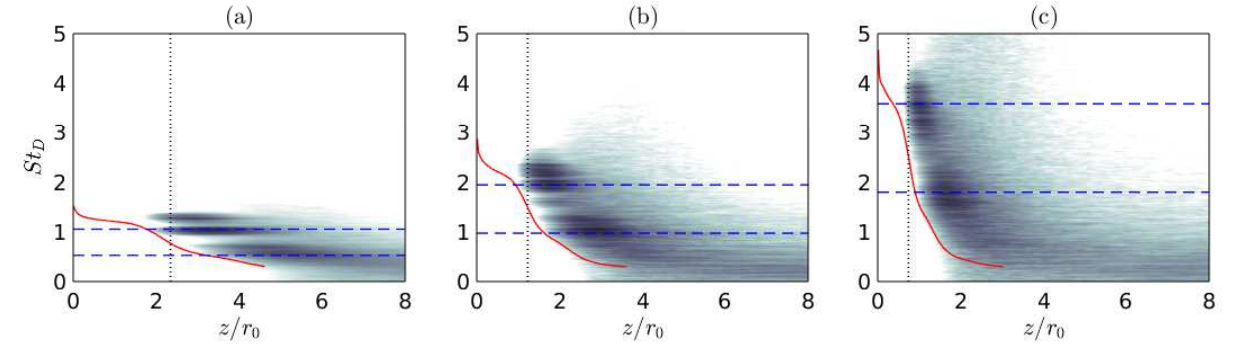

Fig. 4 Power spectral densities of radial velocity fluctuations at $r = r_0$, normalized by their peak values, for the jets with untripped boundary layers with (a) $\delta_{BL} = 0.2r_0$, (b) $\delta_{BL} = 0.1r_0$ and (c) $\delta_{BL} = 0.05r_0$ as a function of z/r_0 and St_D; ——— most unstable frequencies obtained using linear stability analysis for $n_\theta = 0$; – – – values and half the values of the peak frequencies; ····· $z = 100\delta_\theta(0)$. The grey scale ranges logarithmically from 0.05 to 2.

In order to identify the different components in the jet mixing layers, the spectra of radial velocity fluctuations obtained at $r = r_0$ for modes $n_\theta = 0$, 1, and 2 are presented as a function of z/r_0 and St_D in figures 5(a-c) down to $z = 8r_0$ for the jet with $\delta_{BL} = 0.2r_0$, in figures 6(a-c) down to $z = 6r_0$ for $\delta_{BL} = 0.1r_0$ and in figures 7(a-c) down to $z = 4_0$ for $\delta_{BL} = 0.05r_0$. The most unstable frequencies obtained using linear stability analysis and half the values of the peak frequencies in the spectrograms are indicated. The allowable frequency bands for the free-stream upstream-propagating guided jet waves are highlighted by green hatched areas.

In all figures, the most upstream spot of high intensity is located in or very near the band closest to the most unstable frequencies obtained just downstream of the nozzle around $z = 50\delta_\theta(0)$, as it was recently noted for the instability waves

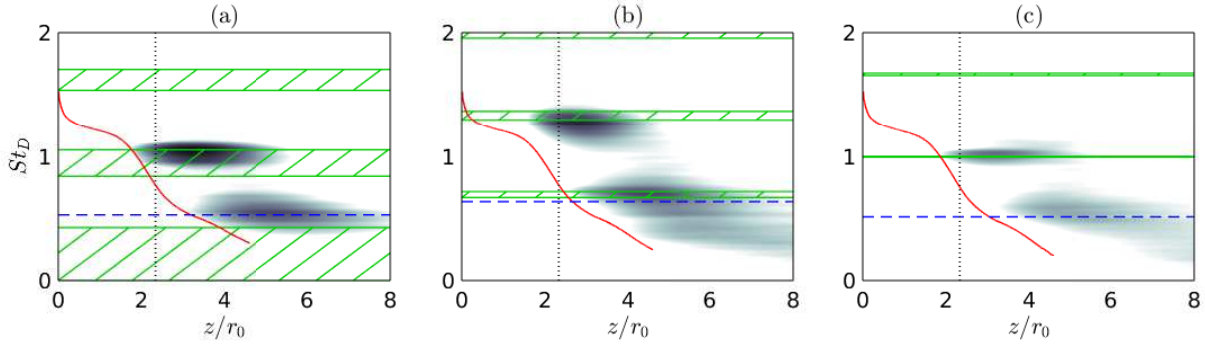

Fig. 5 Power spectral densities of radial velocity fluctuations at $r = r_0$ for the jet with untripped boundary layers with $\delta_{BL} = 0.2r_0$ for (a) $n_\theta = 0$, (b) $n_\theta = 1$ and (c) $n_\theta = 2$ as a function of z/r_0 and St_D; ——— most unstable frequencies predicted using linear stability analysis; – – – half of the peak frequencies; (green hatched areas) ranges of the free-stream upstream-propagating guided jet waves; ····· $z = 100\delta_\theta(0)$. The levels are normalized by the peak values in the full spectra and the grey scale ranges logarithmically from 0.025 to 1.

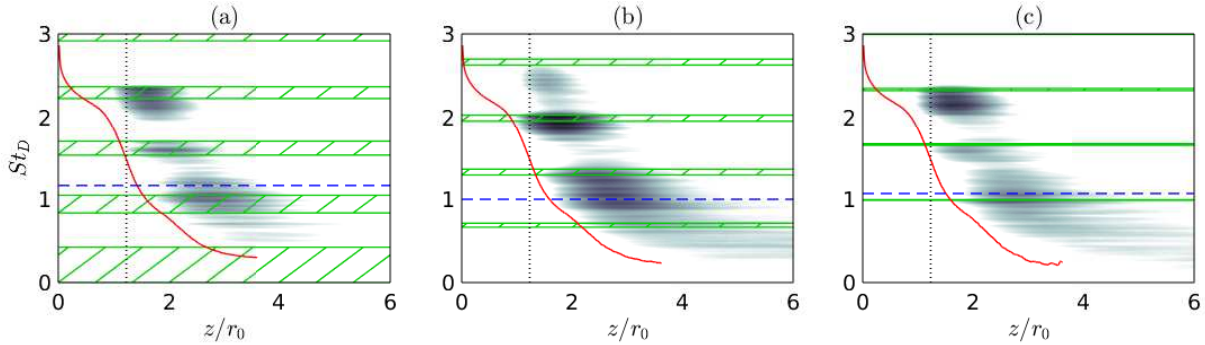

Fig. 6 Power spectral densities of radial velocity fluctuations at $r = r_0$ for the jet with untripped boundary layers with $\delta_{BL} = 0.1r_0$ for (a) $n_\theta = 0$, (b) $n_\theta = 1$ and (c) $n_\theta = 2$ as a function of z/r_0 and St_D; see caption of figure 5 for linetypes, hatches and grayscale.

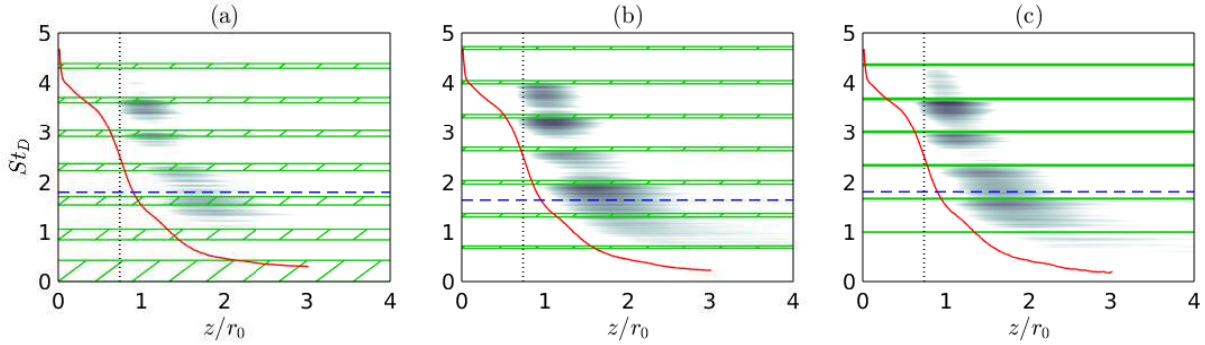

Fig. 7 Power spectral densities of radial velocity fluctuations at $r = r_0$ for the jet with untripped boundary layers with $\delta_{BL} = 0.05r_0$ for (a) $n_\theta = 0$, (b) $n_\theta = 1$ and (c) $n_\theta = 2$ as a function of z/r_0 and St_D; see caption of figure 5 for linetypes, hatches and grayscale.

initially dominating in the jet mixing layers [1]. Farther downstream at $z > 100\delta_\theta(0)$, other spots emerge, especially for thin nozzle-exit boundary layers. They can fall clearly outside the hatched bands, as the second spots in figures 5(a) and 5(c). Their frequencies then correspond to half of the frequencies of the first spots. In most cases, however, they are inside or in the vicinity of the bands, as the several spots in figure 7(c) for instance. Therefore, downstream of the shear-layer rolling-up, high-energy components of two kinds can exist. The first ones consist of velocity fluctuations at the first subharmonic frequencies of the initially dominant, primary instability waves. The second ones result from secondary instability waves excited by free-stream upstream-propagating guided jet waves as the primary ones, but growing at weaker rates and thus emerging farther downstream. Thus, the frequencies and the azimuthal structures of the flow disturbances during the laminar-turbulent flow transition of the present jets are dictated by the properties of the guided jet waves.

The spectra of radial velocity fluctuations obtained at $r = r_0$ for the axial positions $z = z_{peak}$ and $z = z_{peak} + 0.8r_0$ for the jet with $\delta_{BL} = 0.1r_0$ for the azimuthal modes $n_\theta = 0$, 1 and 2 are plotted in figures 8(a-c), as a function of St_D. The first positions are those of the peak values in the spectrograms of figures 6(a-c), giving $z_{peak} = 1.6r_0$ for $n_\theta = 0$ and 2 and $z_{peak} = 1.7r_0$ for $n_\theta = 1$. They are slightly downstream of $z = 100\delta_\theta(0) = 1.23r_0$ and roughly correspond, according to the vorticity field in figure 1(b), to the locations where the vortices first formed in the mixing layers start to interact with one another at the beginning of the vortex-pairing process. The frequency ranges of the free-stream upstream-propagating guided jet waves and half the values of the peak frequencies in the spectrograms are also depicted.

At $z = z_{peak}$, the spectra for $n_\theta = 0$ and for $n_\theta = 1, 2$ are dominated by peaks inside or near the bands associated with the fourth and third radial modes of the guided jet waves, respectively. The peak components are those contained in the first high-energy spots in figures 6(a-c), attributed to the instability waves dominating early on in the jet shear layer [1]. The spectra contain also weaker peaks in the bands for other radial guided jet modes, see the significant levels near the first and second bands in figure 6(c) for $n_\theta = 2$, for instance. These peaks can be related to secondary instability waves excited by the guided jet waves, growing at a lower rate.

Farther downstream, at $z = z_{peak} + 0.8r_0$, the levels in the primary peaks decrease, whereas those in the secondary peaks at lower frequencies do not change much or increase compared with the levels at $z = z_{peak}$, due to the growth, saturation and decay of the instability waves in the axial direction. Significant levels are also visible around half of the peak frequencies, particularly in figures 6(a,b) for $n_\theta = 0$ and 1. They are most likely associated with components generated by nonlinear mechanisms from the primary instability waves as the vortex-pairing process occurs. These results further support the coexistence of velocity disturbances of different nature during the mixing-layer laminar-turbulent transition.

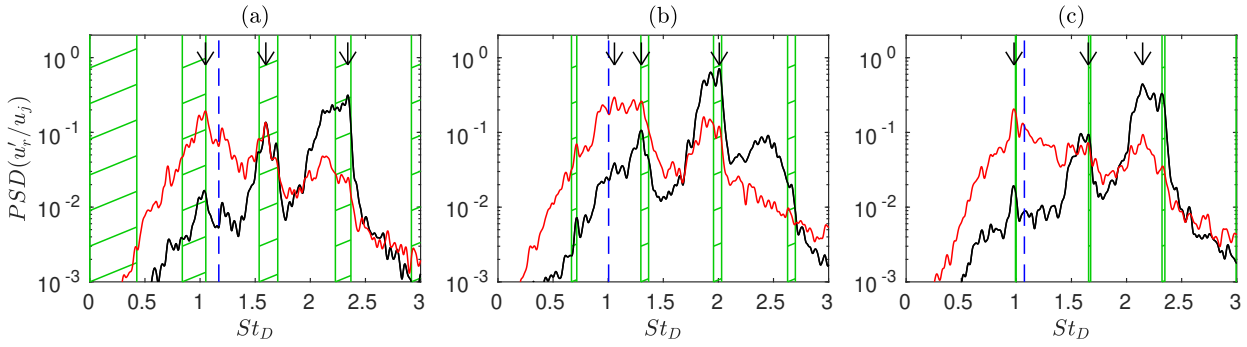

Fig. 8 Power spectral densities of radial velocity fluctuations at $r = r_0$ for the jet with untripped boundary layers with $\delta_{BL} = 0.1r_0$ for (a) $n_\theta = 0$, (b) $n_\theta = 1$ and (c) $n_\theta = 2$ as a function of St_D: ——— at peak location z_{peak} and ——— at $z_{peak} + 0.8r_0$; – – – half of the peak frequencies; (green hatched areas) frequency ranges of the free-stream upstream-propagating guided jet waves; (arrows) frequencies considered in figures 9-11. The levels are normalized as in figure 6(b).

To look for evidence of interactions between upstream-propagating and downstream-propagating waves in the present free jets, as in screeching [26] and impinging [9, 10] resonant jets for instance, the r.m.s. fields of radial velocity fluctuations obtained for the jet with $\delta_{BL} = 0.1r_0$ at the peak frequencies indicated by arrows in figures 8(a-c), namely $\mathrm{St}_D = 1.0490$, 1.596 and 2.3397 for $n_\theta = 0$, $\mathrm{St}_D = 1.0569$, 1.3007 and 2.0080 for $n_\theta = 1$ and $\mathrm{St}_D = 0.9790$, 1.6524 and 2.1459 for $n_\theta = 2$, are represented up to $z = 3r_0$ in figures 9(a-c), 10(a-c) and 11(a-c).

In all cases, very high levels associated with Kelvin-Helmholtz instability waves and turbulent fluctuations are found inside the jet shear layers, as expected. Outside, the results depend on the position of the frequencies considered with respect to the allowable bands of the free-stream upstream-propagating guided jet waves in figures 6(a-c). In all figures except for figure 10(a), for frequencies in or close to the bands, significant levels can be seen in the jet potential core, organized into stripes elongated in the axial direction. The number of stripes varies and increases with the frequency. Standing-wave patterns are also observed on both sides of the shear layer, with wavelength decreasing with the frequency. As explained recently [1], the levels in the potential core and the standing-wave patterns can be attributed to the existence of free-stream upstream-propagating guided jet waves and to their interactions with the Kelvin-Helmholtz instability waves. In this work, these interactions are shown to happen at several frequencies emerging in the velocity spectra on the nozzle lip line, not only at the initially dominant one, and to persist far downstream from the shear-layer rolling-up. Finally, in figure 10(a), for mode $n_\theta = 1$ at a Strouhal number $\mathrm{St}_D = 1.0569$ clearly outside the bands of the guided jet waves in figure 6(b), the levels are negligible in the potential core and no standing-wave patterns are detected in the r.m.s. field. This confirms that the velocity components appearing at that frequency, equal to half of the peak frequency, are not related to the guided jet waves, but are a by-product of the initial instability waves.

2. Jet with tripped boundary layers

Footprints of the guided jet waves are now sought in the mixing layer of the jet with tripped boundary layers. For this jet, due to the high levels of disturbances near the nozzle exit, the r.m.s. values of velocity fluctuations at $r = r_0$ increase monotonically with the axial distance [48, 51] and, near the nozzle exit, the contributions of the first azimuthal modes are not dominant and the spectra are mostly broadband, refer to the results provided in previous papers [20, 33, 34]. As mentioned at the beginning of section III.B, small peaks are, however, found at Strouhal numbers $\mathrm{St}_D = 0.416$ and $\mathrm{St}_D = 0.671$ in the radial velocity spectrum calculated at $z = 0.4r_0$ for the axisymmetric mode [20, 33].

The spectra of the radial velocity fluctuations obtained at $r = r_0$ from the full signals and for the modes $n_\theta = 0$ and 1 between $z = 0$ and $z = 14r_0$, that is from the nozzle-exit section nearly down to the end of the potential core at $z = 14.8r_0$, are presented in figures 12(a-c) as a function of z/r_0 and St_D. The most unstable frequencies predicted using linear stability theory and the frequencies of the acoustic tones in the pressure spectra at $z = 0$ and $r = 1.5r_0$ for $n_\theta = 0$ and 1, characteristic of those of the strongest free-stream upstream-propagating guided jet waves [6, 19, 20], are also shown. Unsurprisingly, the spectra are dominated by broadband components with frequencies decreasing in the axial direction. Peaks are very difficult to distinguish in the full spectra, but may exist in the spectra for $n_\theta = 0$ and 1 for $z \geq 4r_0$. In figure 12(b) for $n_\theta = 0$, in particular, peak components seem to appear around the two Strouhal numbers $\mathrm{St}_D = 0.41$ and 0.67 also emerging at $z = 0.4r_0$ close to the nozzle exit. The first one agrees very well with the Strouhal number $\mathrm{St}_D = 0.4182$ of the first near-nozzle acoustic tone for $n_\theta = 0$, which suggests a link between the free-stream upstream-propagating guided jet waves and the large-scale turbulent structures of the mixing layers far from the nozzle exit.

To further examine the possible presence of peaks in the shear-layer spectra, the spectra of radial velocity fluctuations obtained at $r = r_0$ between $z = 2r_0$ and $z = 10r_0$ every $2r_0$ for modes $n_\theta = 0$ and 1 are plotted in figures 13(a,b) as a function of St_D. They are broadband in all cases and no peaks clearly appear in figure 13(b) for $n_\theta = 1$, indicating that the guided jet waves have a weak influence on the mixing-layer development for the tripped jet, especially compared with the untripped jets. In figure 13(a) for $n_\theta = 0$, however, small peaks are visible at $\mathrm{St}_D \simeq 0.41$ between $z = 4r_0$ and $z = 10r_0$ and at $\mathrm{St}_D \simeq 0.67$ for $z = 4r_0$ and $z = 6r_0$, supporting the comments made above on figure 12(b).

To explore the nature of the two peaks in the spectra for the axisymmetric mode, the r.m.s. fields of radial velocity fluctuations obtained at $\mathrm{St}_D = 0.4182$ and $\mathrm{St}_D = 0.6543$ for $n_\theta = 0$ are represented in figures 14(a,b) for $0 \leq z \leq 12r_0$ and $0 \leq r \leq 6r_0$. The first Strouhal number corresponds to the frequency of the dominant acoustic tone in the acoustic spectra at $z = 0$ and $r = 1.5r_0$ for $n_\theta = 0$, and the second one is the frequency of the local peak at $\mathrm{St}_D \simeq 0.67$ in the spectrum at $z = 6r_0$ in figure 13(a). For $\mathrm{St}_D = 0.4182$, in figure 14(a), strong levels are found in the potential core with no local minimum between $r = 0$ and $r = r_0$. Oscillations resembling standing-wave patterns, highlighted by contour lines, can also be observed at the outer edge of the mixing layer from $z = 0$ down to $z = 12r_0$, with a wavelength $\lambda_{sw} \simeq 2r_0$. Therefore, the free-stream upstream-propagating waves belonging to the first radial guide jet mode existing at the frequency considered interact with the instability waves not only close to the nozzle [1] but also all along the shear layer. These interactions can be expected to affect the turbulent development of the mixing layers of the tripped jet by promoting the formation of coherent large-scale structures. Finally, for $\mathrm{St}_D = 0.6543$, in figure 14(b), the levels are very weak in the potential core. Consequently, guided jet waves cannot be involved in the emergence of components at that frequency in the shear-layer velocity spectra. The origin of these components is currently unexplained.

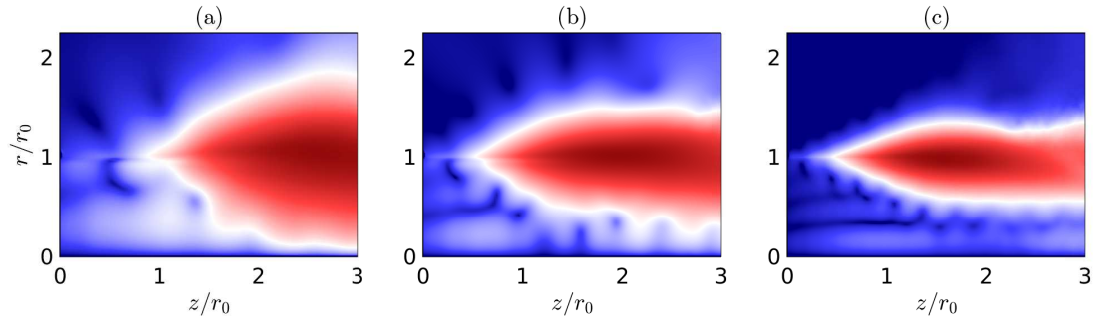

Fig. 9 Power spectral densities of the radial velocity fluctuations for the untripped jet with $\delta_{BL} = 0.1r_0$ for $n_\theta = 0$ at (a) $St_D = 1.0490$, (b) $St_D = 1.5964$ and (c) $St_D = 2.3397$, normalized by their peak values. The colour scale ranges logarithmically from 10^{-7} to 2, from blue to red. The three Strouhal numbers are indicated by arrows in figure 8(a).

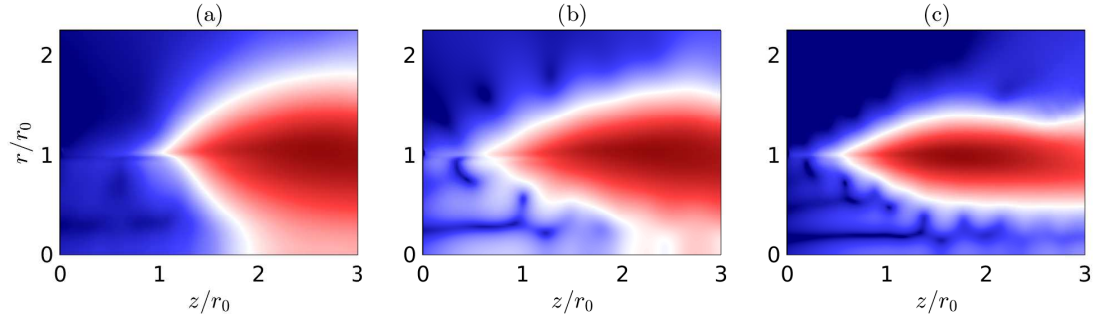

Fig. 10 Power spectral densities of the radial velocity fluctuations for the untripped jet with $\delta_{BL} = 0.1r_0$ for $n_\theta = 1$ at (a) $St_D = 1.0569$, (b) $St_D = 1.3007$ and (c) $St_D = 2.0080$, normalized by their peak values. The colour scale ranges logarithmically from 10^{-7} to 2, from blue to red. The three Strouhal numbers are indicated by arrows in figure 8(b).

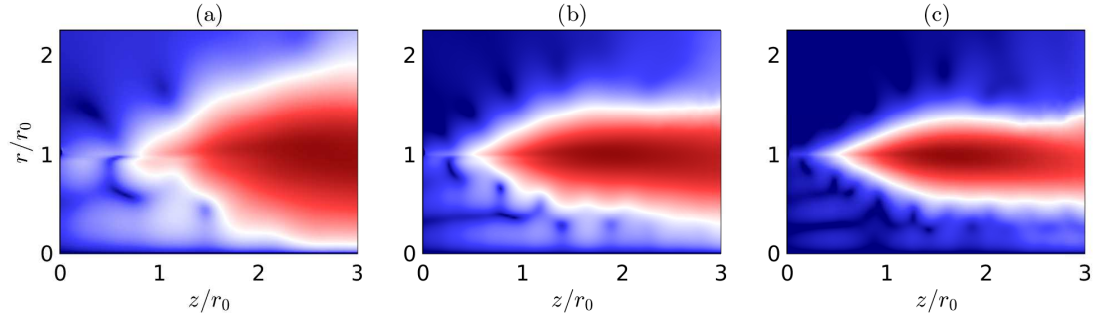

Fig. 11 Power spectral densities of the radial velocity fluctuations for the untripped jet with $\delta_{BL} = 0.1r_0$ for $n_\theta = 2$ at (a) $St_D = 0.9790$, (b) $St_D = 1.6524$ and (c) $St_D = 2.1459$, normalized by their peak values. The colour scale ranges logarithmically from 10^{-7} to 2, from blue to red. The three Strouhal numbers are indicated by arrows in figure 8(c).

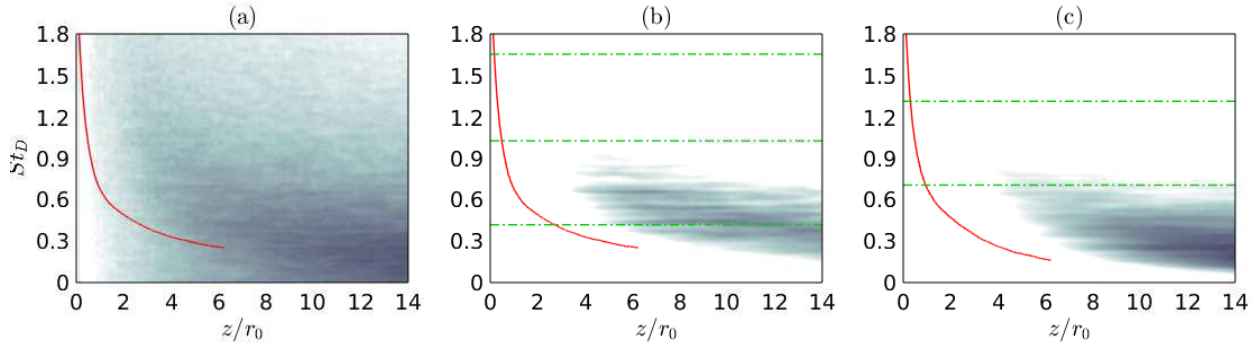

Fig. 12 Power spectral densities of radial velocity fluctuations at $r = r_0$ for the jet with tripped boundary layers as a function of z/r_0 and St_D: (a) full signals, (b) $n_\theta = 0$ and (c) $n_\theta = 1$; ——— most unstable frequencies obtained using linear stability analysis; – · – · – peak frequencies in the pressure spectra at $z = 0$ and $r = 1.5r_0$. The levels are normalized by the peak value in the full spectrum and the grey scales range logarithmically (a) from 0.05 to 2, (b) from 0.01 to 0.1 and (c) from 0.02 to 0.2.

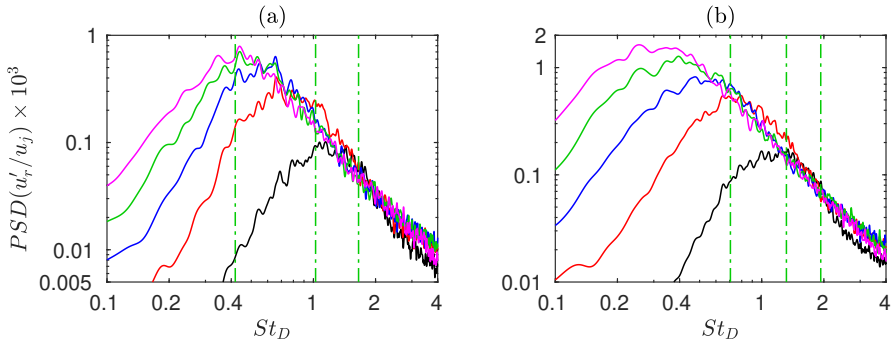

Fig. 13 Power spectral densities of radial velocity fluctuations at $r = r_0$ for the jet with tripped boundary layers for (a) $n_\theta = 0$ and (b) $n_\theta = 1$ as a function of St_D: at ——— $z = 2r_0$, ——— $z = 4r_0$, ——— $z = 6r_0$ ——— $z = 8r_0$ and ——— $z = 10r_0$; – · – · – frequencies of the first three peaks in the pressure spectra at $z = 0$ and $r = 1.5r_0$.

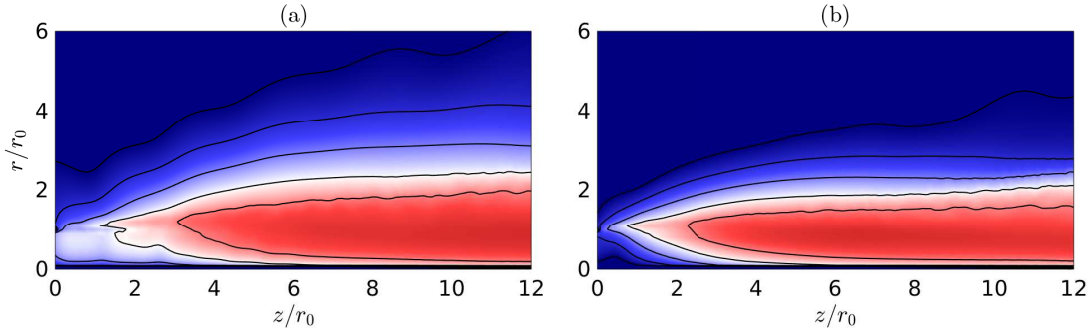

Fig. 14 Power spectral densities of radial velocity fluctuations for the jet with tripped boundary layers for $n_\theta = 0$ at (a) $St_D = 0.4182$ and (b) $St_D = 0.6543$, normalized by their peak values. The colour scale ranges logarithmically from 10^{-5} to 10, from blue to red; the contour levels are equal to 10^{-5}, 10^{-4}, 10^{-3}, 10^{-2} and 10^{-1}.

IV. Conclusion

In the present paper, the effects of the free-stream upstream-propagating guided jet waves on the mixing layers of isothermal free round jets at a Mach number of 0.9 are investigated for three initially fully laminar jets with boundary layers of varying thicknesses and for one initially highly disturbed jet using large-eddy simulations. Different results are found for the two jet initial conditions.

For the initially fully laminar jets, the effects are shown to be very significant and persist all over the laminar-turbulent flow transition region, which can be explained by the high sensitivity of the nozzle-exit velocity profile to the disturbances of small amplitude in this case. They lead to the generation of several strong peak components in the velocity spectra downstream of the nozzle lip and of standing-wave patterns in the r.m.s. velocity fields at both sides of the jet shear layers at the specific frequencies of the free-stream upstream-propagating guided jet waves, as in screeching and impinging resonant jets. These components emerge more or less rapidly depending on the growth rates of the instability waves at these frequencies and can coexist with the subharmonic components of the initially dominating instability waves produced during the first stage of vortex pairings in the shear layers.

For the initially highly disturbed jet, the effects of the guided jet waves on the mixing-layer development are much weaker than for the initially laminar jets, as expected given the nearly turbulent state of the boundary layer at the nozzle exit. For the axisymmetric mode, however, a peak is observed in the velocity spectra along the nozzle lip line several diameters from the nozzle exit and standing-wave patterns can be seen in the r.m.s. velocity field at the outer edge of the jet mixing layer at a Strouhal number $\mathrm{St}_D = 0.41$, corresponding to that of the dominant acoustic tone in the pressure spectra calculated near the jet nozzle and of the strongest free-stream upstream-propagating guided jet waves. Thus, these waves appear to interact with the shear-layer instability waves and may play a role in the formation of coherent large-scale structures in high-subsonic turbulent free jets. This issue will be investigated in future studies.

Acknowledgments

This work was granted access to the HPC resources of PMCS2I (Pôle de Modélisation et de Calcul en Sciences de l'Ingénieur et de l'Information) of Ecole Centrale de Lyon, and P2CHPD (Pôle de Calcul Hautes Performances Dédié) of Université Lyon I, and to the resources of CINES (Centre Informatique National de l'Enseignement Supérieur), IDRIS (Institut du Développement et des Ressources en Informatique Scientifique) and TGCC (Très Grand Centre de calcul du CEA) under the allocation 2021-2a0204 made by GENCI (Grand Equipement National de Calcul Intensif). It was performed within the framework of the LABEX CeLyA (ANR-10-LABX-0060) of Université de Lyon, within the program *Investissements d'Avenir* (ANR-16-IDEX-0005) operated by the French National Research Agency (ANR).

References

[1] Bogey, C., "Interactions between upstream-propagating guided jet waves and shear-layer instability waves in subsonic and nearly ideally expanded supersonic free jets," *J. Fluid Mech.*, 2022. Submitted.

[2] Brès, G. A., and Lele, S. K., "Modelling of jet noise: a perspective from large-eddy simulations," *Phil. Trans. R. Soc. A*, Vol. 377, No. 2159, 2019, p. 20190081. https://doi.org/10.1098/rsta.2019.0081.

[3] Lyrintzis, A. S., and Coderoni, M., "Overview of the use of large-eddy simulations in jet aeroacoustics," *AIAA J.*, Vol. 58, No. 4, 2020, pp. 1620–1638. https://doi.org/10.2514/1.J058498.

[4] Edgington-Mitchell, D., "Aeroacoustic resonance and self-excitation in screeching and impinging supersonic jets - A review," *Int. J. Aeroacoust.*, Vol. 18, No. 2-3, 2019, pp. 118–188. https://doi.org/10.1177/1475472X19834521.

[5] Tam, C. K. W., and Hu, F. Q., "On the three families of instability waves of high-speed jets," *J. Fluid Mech.*, Vol. 201, 1989, pp. 447–483. https://doi.org/10.1017/S002211208900100X.

[6] Towne, A., Cavalieri, A. V. G., Jordan, P., Colonius, T., Schmidt, O., Jaunet, V., and Brès, G. A., "Acoustic resonance in the potential core of subsonic jets," *J. Fluid Mech.*, Vol. 825, 2017, pp. 1113–1152. https://doi.org/10.1017/jfm.2017.346.

[7] Tam, C. K. W., and Ahuja, K. K., "Theoretical model of discrete tone generation by impinging jets," *J. Fluid Mech.*, Vol. 214, 1990, pp. 67–87. https://doi.org/10.1017/S0022112090000052.

[8] Tam, C. K. W., and Norum, T. D., "Impingement tones of large aspect ratio supersonic rectangular jets," *AIAA J.*, Vol. 30, No. 2, 1992, pp. 304–311. https://doi.org/10.2514/3.10919.

[9] Gojon, R., Bogey, C., and Marsden, O., "Investigation of tone generation in ideally expanded supersonic planar impinging jets using large-eddy simulation," *J. Fluid Mech.*, Vol. 808, 2016, pp. 90–115. https://doi.org/10.1017/jfm.2016.628.

[10] Bogey, C., and Gojon, R., "Feedback loop and upwind-propagating waves in ideally-expanded supersonic impinging round jets," *J. Fluid Mech.*, Vol. 823, 2017, pp. 562–591. https://doi.org/10.1017/jfm.2017.334.

[11] Jordan, P., Jaunet, V., Towne, A., Cavalieri, A. V. G., Colonius, T., Schmidt, O., and Agarwal, A., "Jet–flap interaction tones," *J. Fluid Mech.*, Vol. 853, 2018, pp. 333–358. https://doi.org/10.1017/jfm.2018.566.

[12] Tam, C. K. W., and Chandramouli, S., "Jet-plate interaction tones relevant to over-the-wing engine mount concept," *J. Sound Vib.*, Vol. 486, 2020, p. 115378. https://doi.org/10.1016/j.jsv.2020.115378.

[13] Shen, H., and Tam, C. K. W., "Three-dimensional numerical simulation of the jet screech phenomenon," *AIAA J.*, Vol. 40, No. 1, 2002, pp. 33–41. https://doi.org/10.2514/2.1638.

[14] Gojon, R., Bogey, C., and Mihaescu, M., "Oscillation modes in screeching jets," *AIAA J.*, Vol. 56, No. 7, 2018, pp. 2918–2924. https://doi.org/10.2514/1.J056936.

[15] Edgington-Mitchell, D., Jaunet, V., Jordan, P., Towne, A., Soria, J., and Honnery, D., "Upstream-travelling acoustic jet modes as a closure mechanism for screech," *J. Fluid Mech.*, Vol. 855, 2018, p. R1. https://doi.org/10.1017/jfm.2018.642.

[16] Mancinelli, M., Jaunet, V., Jordan, P., and Towne, A., "Screech-tone prediction using upstream-travelling jet modes," *Exp Fluids*, Vol. 60, No. 1, 2019, p. 22. https://doi.org/10.1007/s00348-018-2673-2.

[17] Schmidt, O., Towne, A., Colonius, T., Cavalieri, A. V. G., Jordan, P., and Brès, G. A., "Wavepackets and trapped acoustic modes in a turbulent jet: Coherent structure eduction and global stability," *J. Fluid Mech.*, Vol. 825, 2017, pp. 1153–1181. https://doi.org/10.1017/jfm.2017.407.

[18] Suzuki, T., and Colonius, T., "Instability waves in a subsonic round jet detected using a near-field phased microphone array," *J. Fluid Mech.*, Vol. 565, 2006, pp. 197–226. https://doi.org/10.1017/S0022112006001613.

[19] Brès, G. A., Jordan, P., Jaunet, V., Le Rallic, M., Cavalieri, A. V. G., Towne, A., Lele, S. K., Colonius, T., and Schmidt, O. T., "Importance of the nozzle-exit boundary-layer state in subsonic turbulent jets," *J. Fluid Mech.*, Vol. 851, 2018, pp. 83–124. https://doi.org/10.1017/jfm.2018.476.

[20] Bogey, C., "Acoustic tones in the near-nozzle region of jets: characteristics and variations between Mach numbers 0.5 and 2," *J. Fluid Mech.*, Vol. 921, 2021, p. A3. https://doi.org/10.1017/jfm.2021.426.

[21] Zaman, K. B. M. Q., Fagan, A. F., and Upadhyay, P., "Pressure fluctuations due to 'trapped waves' in the initial region of compressible jets," *J. Fluid Mech.*, Vol. 931, 2022, p. A30. https://doi.org/10.1017/jfm.2021.954.

[22] Bogey, C., "Tones in the acoustic far field of jets in the upstream direction," *AIAA J.*, Vol. 60, No. 4, 2022, pp. 2397–2406. https://doi.org/10.2514/1.J061013.

[23] Michalke, A., "Survey on jet instability theory," *Prog. Aerosp. Sci.*, Vol. 21, 1984, pp. 159–199. https://doi.org/10.1016/0376-0421(84)90005-8.

[24] Morris, P. J., "The instability of high speed jets," *Int. J. Aeroacoust.*, Vol. 9, No. 1-2, 2010, pp. 1–50. https://doi.org/10.1260/1475-472X.9.1-2.1.

[25] Gutmark, E., and Ho, C.-M., "Preferred modes and the spreading rates of jets," *Phys. Fluids*, Vol. 26, No. 10, 1983, pp. 2932–2938. https://doi.org/10.1063/1.864058.

[26] Panda, J., "An experimental investigation of screech noise generation," *J. Fluid Mech.*, Vol. 378, 1999, pp. 71–96. https://doi.org/10.1017/S0022112098003383.

[27] Bogey, C., and Bailly, C., "Influence of nozzle-exit boundary-layer conditions on the flow and acoustic fields of initially laminar jets," *J. Fluid Mech.*, Vol. 663, 2010, pp. 507–539. https://doi.org/10.1017/S0022112010003605.

[28] Camussi, R., and Bogey, C., "Intermittent statistics of the 0-mode pressure fluctuations in the near field of Mach 0.9 circular jets at low and high Reynolds numbers," *Theor. Comput. Fluid Dyn.*, Vol. 35, No. 2, 2021, pp. 229–247. https://doi.org/10.1007/s00162-020-00553-9.

[29] Adam, A., Papamoschou, D., and Bogey, C., "Imprint of vortical structures on the near-field pressure of a turbulent jet," *AIAA J.*, Vol. 60, No. 3, 2022, pp. 1578–1591. https://doi.org/10.2514/1.J061010.

[30] Zaman, K. B. M. Q., "Effect of initial condition on subsonic jet noise," *AIAA J.*, Vol. 23, No. 9, 1985, pp. 1370–1373. https://doi.org/10.2514/3.9094.

[31] Bogey, C., Marsden, O., and Bailly, C., "Large-Eddy Simulation of the flow and acoustic fields of a Reynolds number 10^5 subsonic jet with tripped exit boundary layers," *Phys. Fluids*, Vol. 23, No. 3, 2011, p. 035104. https://doi.org/10.1063/1.3555634.

[32] Bogey, C., Marsden, O., and Bailly, C., "On the spectra of nozzle-exit velocity disturbances in initially nominally turbulent, transitional jets," *Phys. Fluids*, Vol. 23, No. 9, 2011, p. 091702. https://doi.org/10.1063/1.3642642.

[33] Bogey, C., Marsden, O., and Bailly, C., "Influence of initial turbulence level on the flow and sound fields of a subsonic jet at a diameter-based Reynolds number of 10^5," *J. Fluid Mech.*, Vol. 701, 2012, pp. 352–385. https://doi.org/10.1017/jfm.2012.162.

[34] Bogey, C., "Grid sensitivity of flow field and noise of high-Reynolds-number jets computed by large-eddy simulation," *Int. J. Aeroacoust.*, Vol. 17, No. 4-5, 2018, pp. 399–424. https://doi.org/10.1177/1475472X18778287.

[35] Bogey, C., and Sabatini, R., "Effects of nozzle-exit boundary-layer profile on the initial shear-layer instability, flow field and noise of subsonic jets," *J. Fluid Mech.*, Vol. 876, 2019, pp. 288–325. https://doi.org/10.1017/jfm.2019.546.

[36] Mohseni, K., and Colonius, T., "Numerical treatment of polar coordinate singularities," *J. Comput. Phys.*, Vol. 157, No. 2, 2000, pp. 787–795. https://doi.org/10.1006/jcph.1999.6382.

[37] Bogey, C., de Cacqueray, N., and Bailly, C., "Finite differences for coarse azimuthal discretization and for reduction of effective resolution near origin of cylindrical flow equations," *J. Comput. Phys.*, Vol. 230, No. 4, 2011, pp. 1134–1146. https://doi.org/10.1016/j.jcp.2010.10.031.

[38] Bogey, C., and Bailly, C., "A family of low dispersive and low dissipative explicit schemes for flow and noise computations," *J. Comput. Phys.*, Vol. 194, No. 1, 2004, pp. 194–214. https://doi.org/10.1016/j.jcp.2003.09.003.

[39] Bogey, C., de Cacqueray, N., and Bailly, C., "A shock-capturing methodology based on adaptative spatial filtering for high-order non-linear computations," *J. Comput. Phys.*, Vol. 228, No. 5, 2009, pp. 1447–1465. https://doi.org/10.1016/j.jcp.2008.10.042.

[40] Berland, J., Bogey, C., Marsden, O., and Bailly, C., "High-order, low dispersive and low dissipative explicit schemes for multiple-scale and boundary problems," *J. Comput. Phys.*, Vol. 224, No. 2, 2007, pp. 637–662. https://doi.org/10.1016/j.jcp.2006.10.017.

[41] Tam, C. K. W., and Dong, Z., "Radiation and outflow boundary conditions for direct computation of acoustic and flow disturbances in a nonuniform mean flow," *J. Comput. Acous.*, Vol. 4, No. 2, 1996, pp. 175–201. https://doi.org/10.1142/S0218396X96000040.

[42] Bogey, C., and Bailly, C., "Large Eddy Simulations of transitional round jets: influence of the Reynolds number on flow development and energy dissipation," *Phys. Fluids*, Vol. 18, No. 6, 2006, p. 065101. https://doi.org/10.1063/1.2204060.

[43] Fauconnier, D., Bogey, C., and Dick, E., "On the performance of relaxation filtering for large-eddy simulation." *J. Turbulence*, Vol. 14, No. 1, 2013, pp. 22–49. https://doi.org/10.1080/14685248.2012.740567.

[44] Kremer, F., and Bogey, C., "Large-eddy simulation of turbulent channel flow using relaxation filtering: Resolution requirement and Reynolds number effects," *Comput. Fluids*, Vol. 116, 2015, pp. 17–28. https://doi.org/10.1016/j.compfluid.2015.03.026.

[45] Bogey, C., "A database of flow and near pressure field signals obtained for subsonic and nearly ideally expanded supersonic free jets using large-eddy simulations," https://hal.archives-ouvertes.fr/hal-03626787, 2022.

[46] Fontaine, R. A., Elliott, G. S., Austin, J. M., and Freund, J. B., "Very near-nozzle shear-layer turbulence and jet noise," *J. Fluid Mech.*, Vol. 770, 2015, pp. 27–51. https://doi.org/10.1017/jfm.2015.119.

[47] Bogey, C., "Generation of excess noise by jets with highly disturbed laminar boundary-layer profiles," *AIAA J.*, Vol. 59, No. 2, 2021, pp. 569–579. https://doi.org/10.2514/1.J059610.

[48] Bradshaw, P., "The effect of initial conditions on the development of a free shear layer," *J. Fluid Mech.*, Vol. 26, No. 2, 1966, pp. 225–236. https://doi.org/10.1017/S0022112066001204.

[49] Browand, F. K., and Latigo, B. O., "Growth of the two-dimensional mixing layer from a turbulent and nonturbulent boundary layer," *Phys. Fluids*, Vol. 22, No. 6, 1979, pp. 1011–1019. https://doi.org/10.1063/1.862705.

[50] Zaman, K. B. M. Q., and Hussain, A. K. M. F., "Vortex pairing in a circular jet under controlled excitation. Part 1. General jet response." *J. Fluid Mech.*, Vol. 101, No. 3, 1980, pp. 449–491. https://doi.org/10.1017/S0022112080001760.

[51] Husain, Z. D., and Hussain, A. K. M. F., "Axisymmetric mixing layer: influence of the initial and boundary conditions," *AIAA J.*, Vol. 17, No. 1, 1979, pp. 48–55. https://doi.org/10.2514/3.61061.